Islamic University Journal of Applied Sciences (IUJAS)
https://journals.iu.edu.sa/jesc

Volume VII, Issue II, December 2025, Pages 91-100

Interaction of Chimney Plumes with an Isolated Obstacle: Experimental and Computational Study

Nejla Mahjoub Said *, Halemah Ibrahim Elsaeedy, Magda Abd El-Rahman, Fethi Mohamed Maiz

Department of Physics, College of Science, King Khalid University, Abha 61413, Saudi Arabia
nalmahjoub@kku.edu.sa, halsayede@kku.edu.sa, majedah@kku.edu.sa, fmaiz@kku.edu.sa

*Corresponding author: (Nejla Mahjoub Said), *Email Address*: nalmahjoub@kku.edu.sa

Abstract

This study investigates the dispersion of pollutants emitted from a chimney in the vicinity of a three-dimensional rectangular building. In the experimental part, a wind tunnel setup was used, where tracer discharges (air seeded with glycerin particles) were continuously released from a point source located within a regular array of building-like obstacles. Measurements of mean velocity and turbulence parameters were obtained. Particle Image Velocimetry (PIV) was employed to capture both instantaneous and mean dynamic characteristics. In the numerical part, the proposed model simulates the flow dynamics and heat transfer using the three-dimensional Reynolds-averaged Navier–Stokes (RANS) equations with an RSM turbulence closure model. The comparison between experimental and numerical results shows a high level of agreement. A comprehensive analysis was conducted to assess the influence of wind velocity on pollutant dispersion from the chimney around the building and its surroundings.

Keywords: Experimental Study; Numerical Simulation; Obstacle; Recirculation Zone.

https://doi.org/10.63070/jesc.2025.024
Received 15 June 2025; Revised 25 August 2025; Accepted 18 September 2025.
Available online 12 October 2025.
Published by Islamic University of Madinah on behalf of ***Islamic University Journal of Applied Sciences.***

1. Introduction

With urban and industrial growth, air pollution has become a major concern for organizations working to improve environmental conditions. Protecting air quality in cities requires understanding how pollutants spread and disperse, whether they are gases, particles, liquids, or even noise. In the case of gaseous emissions, factors such as building density, street geometry, and layout play a key role in how pollutants move. Regulations aim to keep emissions low enough to minimize their impact on the environment. At the local scale, the presence of buildings strongly influences airflow. Obstacles such as towers or street canyons create recirculation zones that trap pollutants and lead to high, uneven concentrations. Our focus is on this scale, studying how different building shapes cylindrical, rectangular, or parallelepiped affect the surrounding airflow and turbulence. The flow field is complex, especially when rough urban surfaces interact with environmental winds. Earlier research often simplified the problem, either by ignoring pollutant sources or by studying dispersion over flat terrain without considering buildings. To capture these dynamics more realistically, we use a 2D block-structured hexahedral mesh with FLUENT. Different turbulence models are applied (standard k–ε, k–ω, and Reynolds Stress Transport) to simulate the flow. Previous studies have also highlighted the importance of building shape and wind direction. For example, Liu et al. [1] used LES to model pollutant transport in street canyons, showing its effectiveness for predicting dispersion in crowded areas. Lateb et al. [2] studied roof-stack emissions near towers, analyzing the effect of stack height and exhaust velocity. Gausseau et al. [3] examined how wind direction changes dispersion from building-mounted stacks, while Sivanandan et al. [4] investigated how temperature gradients and stack orientation influence plume rise and spread. Turbulence was modeled using the realizable k–ε approach in FLUENT. In inline stack configurations, the upwind plume shields the one behind it, allowing for greater plume rise under the same temperature gradient. Compared to angled or staggered setups, the inline case also shows stronger plume oscillations. Several experimental and numerical studies help shed light on these dynamics. Mahjoub et al. [5,6] used Particle Image Velocimetry (PIV) to study coherent structures in the wake of a circular jet from a stack in crossflow, focusing on regions near the chimney tip. In another study, Mahjoub et al. [7] examined flow around 3D rectangular obstacles in a wind tunnel, testing different angles of attack. Contini et al. [8] showed that the Reynolds number of the stack flow can strongly influence plume trajectories in small-scale experiments. Other researchers looked at building effects. Saathoff et al. [9] studied how rooftop structures change dispersion from rooftop stacks, while Castro et al. [10] compared experiments with LES and DNS, finding LES gives excellent agreement. Fuka et al. [11] investigated scalar dispersion in building arrays, showing how even slight shifts in wind direction can alter pollutant spread. Amamou et al. [12]

explored chimney emissions near a cylindrical obstacle in a wind tunnel, combining PIV experiments with RSM simulations. Their results confirmed that wind speed and obstacle presence strongly affect the velocity, temperature, and concentration fields. We carried out a wind tunnel experiment to study how airflow interacts with an obstacle, using Particle Image Velocimetry (PIV). Different wind speeds were tested to measure flow behavior, especially turbulence near the obstacle. The experimental results were then compared with numerical simulations based on the Reynolds Stress Model (RSM). Once validated, the model was used to examine how obstacle position affects the flow.

2. Experimental set-up

The experiments were performed in a 3 m-long wind tunnel with a 0.2 m × 0.5 m test section. The jet was produced by a smooth iron pipe, 0.1 m long and 10 mm in diameter, connected to the main air supply and discharging air at constant temperature. An isolated rectangular obstacle and the chimney were both positioned along the central vertical plane of the tunnel (Figure 1). Flow measurements combined Particle Image Velocimetry (PIV) to capture instantaneous and mean velocity fields with hot-wire anemometry to validate the cross-flow velocity. To minimize boundary effects, the setup was placed about 2.9 m upstream of the tunnel exit. The cross-flow was generated by motors at the tunnel entrance, with velocities limited to 12 m/s from the lower inlet section. To visualize mixing, glycerin particles were added to the chimney jet. PIV measurements were carried out using a TSI PowerView system, and the averaged fields were obtained from 500 successive acquisitions.

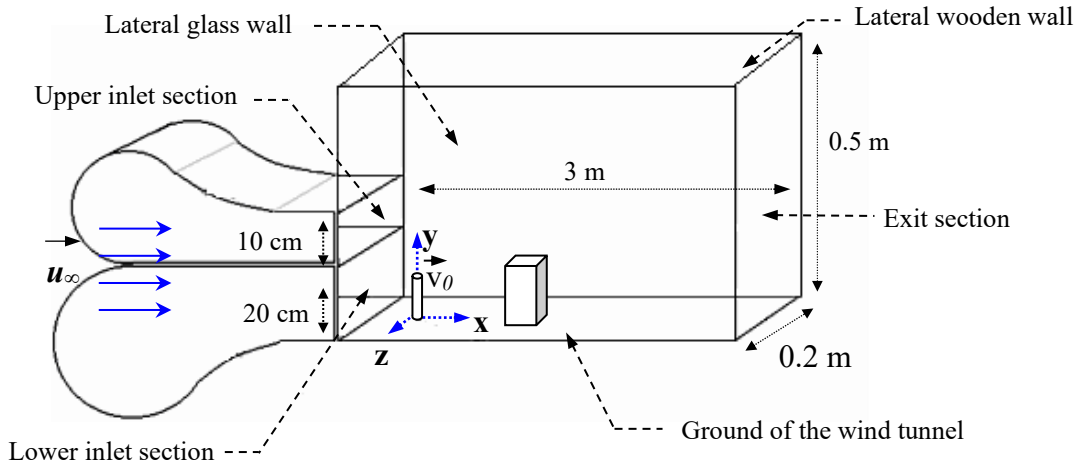

Figure 1. The emplacement of the chimney, obstacle and the Cartesian coordinate system in the wind tunnel

3. Computational set-up

The average flow field around the stack and the rectangular obstacle at ground level was simulated under steady, three-dimensional, turbulent conditions. The numerical approach follows the

methodology of Mahjoub et al. [5], first validating the model and then introducing additional conditions to better capture real flow behavior. The governing equations include conservation of mass, momentum, energy, and species transport, expressed in Cartesian coordinates and solved using Favre's decomposition. To close the system, the Reynolds Stress Model (RSM) was adopted, as it accounts for the effects of turbulence through second-order closure. The main modeled terms include molecular diffusion, turbulence production, turbulent diffusion, buoyancy effects, pressure strain, and dissipation.

Equations for turbulent kinetic energy (k) and its dissipation rate (ε) were also solved. The boundary conditions applied to the system are summarized in Table 1.

Table 1. Boundary condition.

Boundaries	Velocity (m/s)	Temperature (K)	Mass Fraction	Kinetic energy m^2/s^2	Rate of dissipation $m^2\ s^{-3}$
Chimney	$\tilde{u} = u_0, \tilde{v} = 0, \tilde{w} = 0$	$\tilde{T} = T_0$	$\tilde{f} = f_0$	$k_0 = 10^{-3}u_0^2$	$\varepsilon = k_0^{\frac{3}{2}}/0.5d$ [13]
Crossflow	$\tilde{u} = u_\infty, \tilde{v} = 0, \tilde{w} = 0$	$\tilde{T} = T_\infty$	$\tilde{f} = 0$	$k_\infty = 5.10^{-3}u_\infty^2$	$\varepsilon = k_0^{\frac{3}{2}}/0.2H_T$ [13]
Obstacles and ground	$\tilde{u} = 0, \tilde{v} = 0, \tilde{w} = 0$	$\partial\tilde{T}/\partial n = 0$	$\partial\tilde{f}/\partial n = 0$	$k = 0$	$\partial\varepsilon/\partial y = 0$
Other boundaries of the domain	$\frac{\partial\tilde{u}}{\partial n} = 0, \frac{\partial\tilde{v}}{\partial n} = 0, \frac{\partial\tilde{w}}{\partial n} = 0$	$\partial\tilde{T}/\partial n = 0$	$\partial\tilde{f}/\partial n = 0$	$\partial k/\partial n = 0$	$\partial\varepsilon/\partial n = 0$

Running the numerical simulation posed several challenges. The flow structure required very fine meshing across much of the domain. To capture the details, especially around the chimney, the obstacle, and the ground, we used a non-uniform grid with denser cells in these regions (standard wall functions applied). Overall, the mesh remained very fine in a large part of the domain (Table 2).

Table 2. Grid steps in the different locations of the domain.

Direction		Δ	α_x	Δy	Δz
Longitudinal	Upstream of the chimney	0.008	0.98		
$x_{i+1} = x_i + \alpha_x\Delta$	Near the chimney and the obstacle	0.001	1		
	Downstream of the obstacle	0.006	0.98		
Transverse	Near the ground			0.001	
	As we move away, the step of calculation increases gradually			0.003	
	Step of calculation increases gradually			0.007	
Lateral					0.004

The grid was refined between the elevated jet and the obstacle (Figure 2) to better capture flow details. We tested three grids: a coarse one (216 × 130 × 35), a finer one (250 × 145 × 40), and a very fine one (250 × 155 × 50) with more cells in the vertical and lateral directions. The final computations were carried out with the finest grid (250 × 155 × 50), since grid-independence tests showed that the difference from the medium grid was less than 5%. This confirms that the chosen mesh provides grid-independent results.

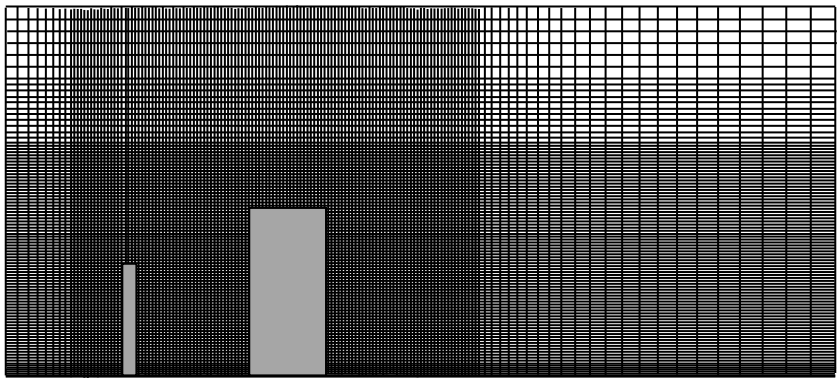

Figure 2. Computational grid on the median plane

4. Results and discussion

Laboratory experiments are a valuable tool for studying pollution dispersion. They provide scaled-down insights that can be applied to real situations, complementing other approaches such as field observations, analytical models, and numerical simulations. Each method has its strengths and limitations, but together they help clarify the mechanisms involved. In Figure 3, we examined how the distance between the chimney and the obstacle affects plume behavior. Two cases were tested: one where the distance equals three times the chimney height, and another where it equals twice the chimney height. The obstacle height was fixed at 9 cm, with both wind and ejection velocities set to 8 m/s. Results show that the plume impact is stronger when the obstacle is placed farther away (three times the chimney height). This is expected, as the plume spreads conically with distance from the chimney. The velocity ratio here is 1.

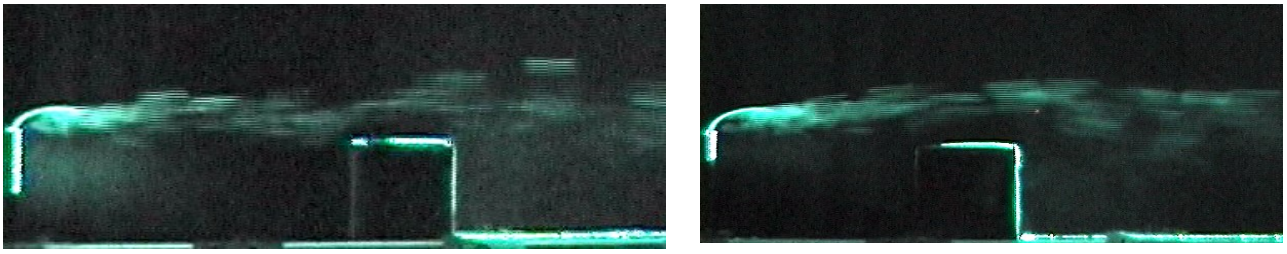

Figure 3. Plume evolution around an obstacle for a velocity ratio equal to 1 and for two gaps from the source (20 cm, 30 cm) v_0 = 8 m/s, u_∞= 8 m/s

In Figure 4, the obstacle height was varied (h_b = 6 cm and h_b = 9 cm) while keeping its distance from the 10 cm chimney fixed at 20 cm. When h_b = 9 cm, the plume rises, bends, and flows over the obstacle. For h_b = 6 cm, the plume clears the obstacle without direct contact.

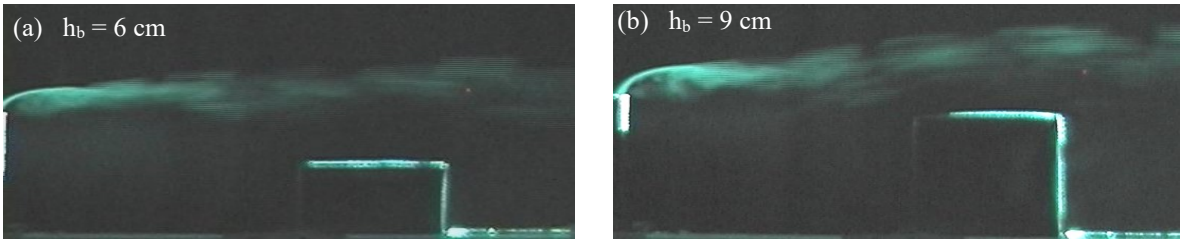

Figure 4. Effect of obstacle height, v0= 8 m/s, u∞= 8 m/s

Figure 5 shows the plume in the horizontal plane through the chimney exit (xz-plane). The results indicate that the flow is not purely two-dimensional, as vortices and lateral bypasses appear near the chimney, revealing non-zero velocity along the z-direction. When the wind tunnel flow exceeds the plume velocity (Fig. 5a), the plume behaves passively, simply following the transverse wake created behind the chimney similar to the wake of a cylinder. This wake-like structure persists even when the crossflow velocity is lower (Fig. 5b).

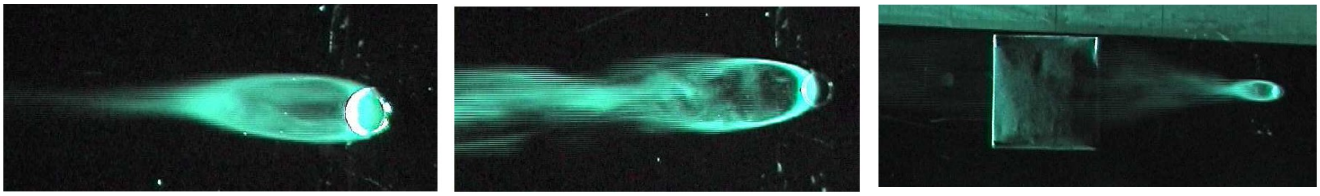

(a) Wind velocity greater than ejection velocity v_0= 8m/s, u_∞=12 m/s

(b) The wind velocity is equal to the ejection velocity v_0= 8 m/s, u_∞= 8 m/s

c) Wind velocity equal to the ejection velocity (R=), Distance chimney-obstacle=20 cm, h_b=6 cm

Figure 5. Visualization of the plume in a horizontal plane

At the chimney exit, turbulent structures known as Kelvin–Helmholtz instabilities appear (Figure 6, for R=∞, 5.4, 1.4, and 0.7).

u_∞ = 0 m/s (R = ∞)

u_∞ = 0.25 m/s (R = 5.4)

u_∞ = 0.95 m/s (R = 1.4)

u_∞ = 2 m/s (R = 0.7)

Figure 6. Experimental visualization of the influence of the external flow near the chimney exhaust, v0 = 1.35 m/s

These arise when two fluid layers moving at different speeds interact, forming a vortex sheet at their boundary. The rotation of these vortices depends on the velocity ratio between the jet and the wind (v_0/u_∞). To study this effect, we considered four velocity ratios. When R = ∞ (no wind), the jet expands freely outward. With external flow added (R = 5.4, 1.4, and 0.7), the shear layer changes direction: clockwise when the jet dominates, and counterclockwise when the wind prevails.

The experimental setup was reproduced numerically to ensure consistency. We modeled a 3D isothermal jet flow in a steady turbulent regime ($T\infty$ = 293.15 K, v_0 = 8 m/s, Re_d = 5128). Figure 7 compares experimental and numerical results obtained with the second-order turbulence model, focusing on the longitudinal and vertical mean velocity components. At x = 0.05 m (between the chimney and the obstacle) and x = 0.125 m (on the obstacle roof), the longitudinal velocity shows clear disturbances caused by the building, with results matching the experiments well. For the vertical velocity, profiles at the same locations confirm this agreement. At x = 0.05 m, the vertical velocity is higher than at x = 0.125 m, indicating that the obstacle slows the flow. The section above the roof shows two peaks, reflecting a recirculation zone and negative velocities just above the surface. Overall, the RSM turbulence model reproduces the main features of pollutant dispersion around buildings under different wind conditions with good accuracy.

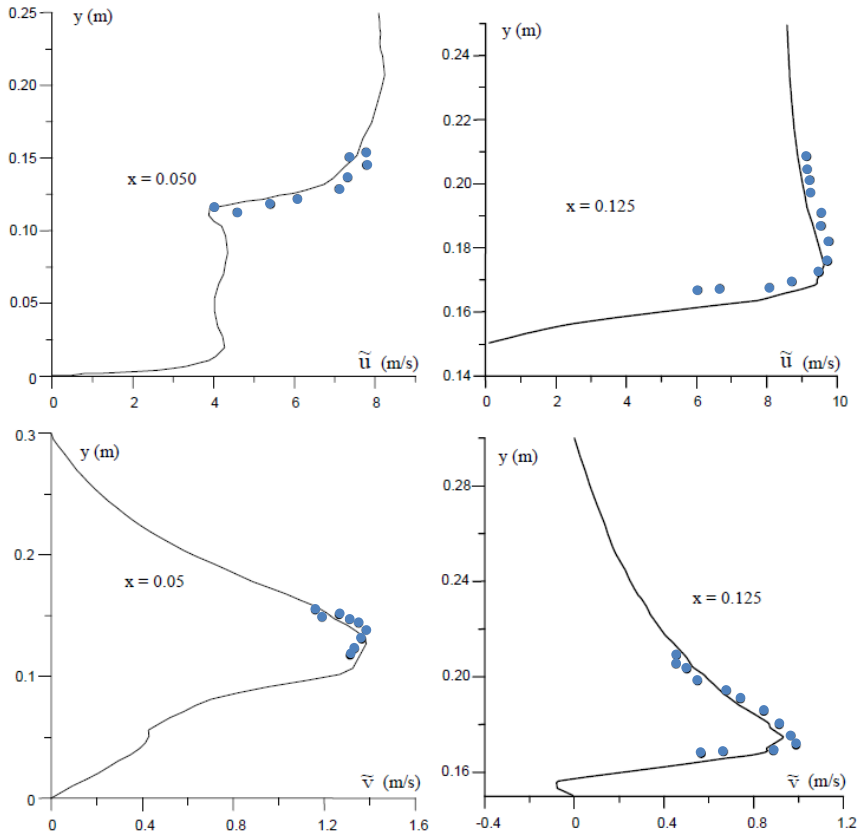

Figure 7. Mean longitudinal $\tilde{u}$ and normal $\tilde{v}$ velocity profiles at v_0 = 8 m/s and u_∞ = 8 m/s

Figure 8 presents the longitudinal and vertical velocity profiles along the normal coordinate *y* at different positions (*x*= 0.20, 0.30, 0.35, and 0.40m) in the recirculation zone. Downstream of the obstacle, the negative velocity values confirm the presence of recirculation. The longitudinal velocity shows two peaks: the upper peak corresponds to the pollutant jet trajectory, while the lower peak results from fluid passing through the wake near the ground. Both peaks decrease with distance downstream. Recirculation is clear at *x*=0.20m and *x*=0.30m, but nearly absent at *x*=0.40m.

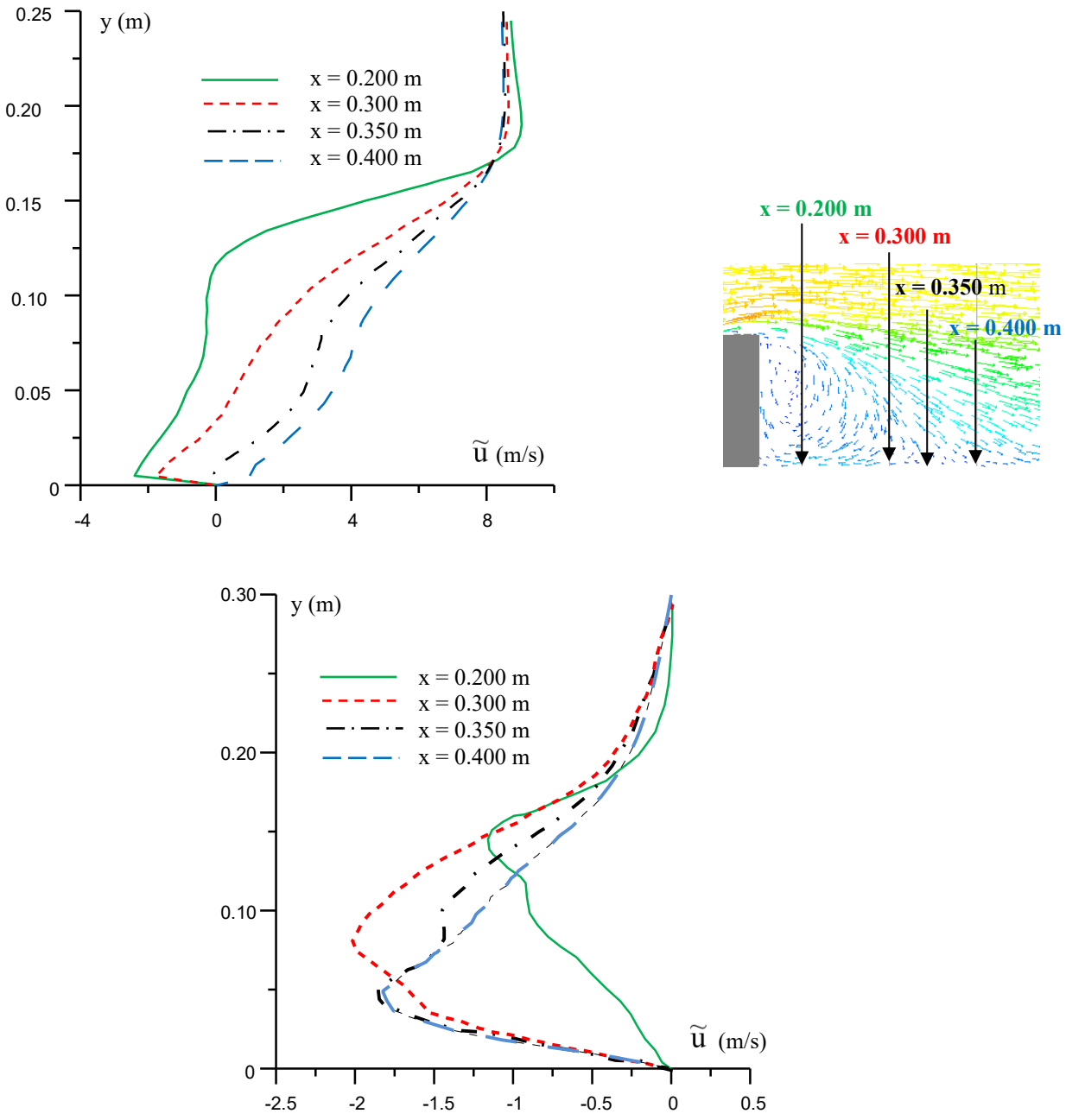

Figure 8. Velocity profiles behind the obstacle (in the recirculation zone) v_0= 8 m/s , u_∞= 8 m/s

5. CONCLUSION

Our paper presents both experimental and numerical investigations to better understand the interaction between a continuous plume emitted from a chimney and a nearby building under varying wind velocities. The experiments were conducted using Particle Image Velocimetry (PIV), while the numerical simulations employed the Reynolds Stress Model (RSM) for turbulence. All collected data have been thoroughly validated. The agreement between the wind tunnel measurements and the numerical results, using identical inlet boundary conditions, was quite good. Key flow features, particularly the large vortex structures, were predicted very accurately. Plume dispersion was also analyzed using digital image techniques, and the turbulent dispersion model describing pollutant spread is presented.

The most significant findings of our study can be summarized as follows:

- The presence of a building behind the stack strongly affects the flow structure.
- Differences in height between the stack and the building modify the plume pattern.
- Higher wind speeds cause the plume to spread further before reaching ground level.
- At low wind speeds, the plume tends to rise more vertically due to the greater momentum difference between the released pollutant and the incoming wind.

5. References

[1] Liu, Y.S.; Cui, G.X.; Wang, Z.S.; Zhang, Z.S. Large eddy simulation of wind field and pollutant dispersion in downtown Macao. Atmos. Environ. 45 (2011) 2849–2859.

[2] Lateb M. ; Masson C. ; Stathopoulos T. ; Bedard C. Effect of stack height and exhaust velocity on pollutant dispersion in the wake of a building, Atmospheric Environment. 45, 29 (2011) 5150-5163

[3] Gousseau, P.; Blocken, B.; Stathopoulos, T.; van Heijst, G.J.F. Near-field pollutant dispersion in an actual urban area: Analysis of the mass transport mechanism by high resolution Large Eddy Simulations. Comput. Fluids 114 (2015) 151–162.

[4] Sivanandan H.; Ratna K. V.;·Goel M.; Asthana A. A study on plume dispersion characteristics of two discrete plume stacks for negative temperature gradient conditions, Environmental Modeling & Assessment 26 (2021) 405–422

[5] Mahjoub Said N.; Mhiri H.; Le Palec G.; and Bournot Ph. Experimental and numerical analysis of pollutant dispersion from a chimney. Atmospheric Environment. 39 (2005) 1727-1738.

[6] Mahjoub Said N.; Habli S.; Mhiri H.; Le Palec G.; Bournot H. Flow field measurement in crossflowing elevated jet. ASME Journal of Fluids Engineering. 129 (2007) 551-562.

[7] Mahjoub Said N.; Mhiri H.; Caminat P.; Le Palec G.; Bournot Ph. Wind tunnel investigation and numerical simulation of the near wake dynamics for rectangular obstacles. Environmental Engineering Science. 25 (2008) 1037-1060.

[8] Contini D.; Cesari D.; Donateo A.; Robins A. G. Effects of Reynolds number on stack plume trajectories simulated with small scale models in a wind tunnel. Journal of Wind Engineering & Industrial Aerodynamics. 97 (2009) 468-474

[9] Saathoff P.; Amit G.; Ted S.; Louis L. Contamination of Fresh Air Intakes Due to Downwash from a Rooftop Structure. Journal of the Air & Waste Management Association. 59 (2009) 343-353.

[10] Castro I. P.; Xie Z. T.; Fuka V.; Robins A. G.; Carpentieri M.; Hayden P.; Hertwig D.; Coceal O. Measurements and Computations of Flow in an Urban Street System. Boundary-Layer Meteorology. 162 (2017) 207–230.

[11] Fuka V.; Xie Z. T.; Castro I. P.;·Hayden P.; Carpentieri M.; Robins A. Scalar Fluxes Near a Tall Building in an Aligned Array of Rectangular Buildings. Boundary-Layer Meteorology. 167 (2018) 53–76

[12] Amani A.; Amira A.; Rim B. K.; Nejla M. S. Numerical parametric study of turbulent counterflowing jets. International Communications in Heat and Mass Transfer. 155 (2024) 107526.

[13] Demuren A. O.; Rodi W. Three Dimensional Numerical Calculations of Flow and Plume Spreading Past Cooling Towers. ASME J. Heat Transfer. 109 (1987) 113–119.